

Ordering of atomic mono-layers on a (001) cubic crystal surface

Laurent Proville

Groupe de Physique des Solides, UMR 7588-CNRS

Universités Paris 7 & Paris 6, Tour 23, 2 pl. Jussieu 75251, Paris Cedex 05, France

(October 28, 2018)

The self-organization of a chemi-sorbed mono-layer is studied as a two dimensional ordering process in presence of surface stress. As proved previously for a single phase separation, a steady surface state is yielded from the competition between the domain boundary energy and the surface stress elastic energy. In the present letter, the resulting patterns are shown to depend on the interplay between the symmetries of both the internal layer order and the underlying crystal. For experimental relevance, our study is focussed on a (001) copper surface and we believe to enhance a route to stabilize novel surface nanostructures.

The growth of nanostructure onto solid surfaces provides us with promising technical perspectives for the electronic miniaturization as for the heterogeneous catalyzer assembling. The mono-layer self-organization (SO) on crystal surface is an efficient mean to control the nanostructure growth by constructing a template with regular nanometer sizes and spacings. The matter which may be deposited subsequently on this template is likely to organize with same patterns as the mono-layer.

Recent analysis of chemisorbed mono-layers on (001) Copper surfaces, via Scanning Tunneling Microscopy (STM) [1–3] and Spot Profile Analyzing Low Energy Electron Diffraction (SPA-LEED) [4] showed both a large panel of morphologies and the means to control their formations.

The interplay between the long range elastic interaction yielded by the underlying crystal surface stress and the domain boundary energy has been well known to control the surface SO since the papers of Marchenko [5] and Vanderbilt *et al.* [6,7]. While Refs. [5,6] address the cases of the vicinal surfaces and the surface reconstruction, Ref. [7] was performed in the very general context of a two-phase system with $1/r^3$ isotropic dipolar interactions in two dimensions and thus the latest study is now used to get an insight into the chemisorbed mono-layer SO. Indeed, considering an assembly of surface domains inside which are fixed adatoms, the energy cost due to the boundary, i.e., where the adatom environment is unfavorable, is proportional to the total boundary length L , i.e., $L \times L$. As for a given coverage L is minimum for a single compact domain, the smaller is the number of compact domains, the weaker will be the domain boundary energy. On the other hand, if a non-negligible crystal surface stress Λ is associated with the adatoms adsorption, the surface stress inhomogeneities induce some forces that are located at the domain boundaries. These forces yield a crystal strain and thus an elastic work is involved which is minimum when the forces are separated by a distance as large as possible. So the surface ground state structure should balance the twice aforementioned opposite features and the calculations of [5–7] proved that periodic domains occur with a period selection which increases exponentially with the ratio L/Λ^2 , with a suitable multiplier which depends on the material elastic constants.

In Ref. [8], a 2-dimensional spinodal theory was proved to be an efficient tool to study the SO kinetics on a (001) cubic crystal surface provided the elastic anisotropy due to the underlying crystal symmetries is taken into account in the calculation of the total free energy F . The 2D Cahn-Hilliard equation was assumed to drive the surface diffusion of the adatoms, i.e., the time evolution of the local adatom coverage θ is given by:

$$\frac{\partial \theta(\mathbf{r}, t)}{\partial t} = M_\theta \Delta \frac{\delta F}{\delta \theta(\mathbf{r}, t)} \quad (1)$$

A complete analysis of this equation can be found in Refs. [9,10] with no elastic interactions, indeed. The approach

developed in Ref. [8] was actually devoted to study a single phase separation on a crystal surface, no matter how the internal layer order may play a role. In what follows, we describe how to take into account the layer symmetries of both the adatom layer and the underlying cubic crystal. These features are proved to determine the surface patternings. We present the different layer nanostructures and enhance the control parameters both for the size and the shape of those structures. Comparison with experiments is also proposed as an example of how to interpret our results.

Some additional order parameters (OP), noted η_j are required to describe ordered phases that may coexist with either orientational or translational variants. The kinetics is thus completed by a set of Allen-Cahn (also known as time dependant Ginzburg-Landau) equations:

$$\frac{\partial \eta_j(\mathbf{r}, t)}{\partial t} = -M_\eta \frac{\delta F}{\delta \eta_j(\mathbf{r}, t)} \quad (2)$$

that control the time evolution of each non-conserved η_j . Such approach was developed in metallurgical science by Khachatryan [11] for the microstructure ordering in alloys. The mobility constant M_θ is proportional to the Fick diffusion coefficient which is around $10^{-6} \text{cm}^2/\text{s}$ at 300 K (see [12]). As we found no experimental results about the ordering kinetics of surface, M_η is an adjustable parameter which is assumed to fulfill the adiabatic regime, i.e., the ordering kinetics is much faster than the matter diffusion.

The total surface free energy F can be written as a sum of two terms, i.e., first a chemical term F_{chem} which includes both the energy due to covalent bounds between the substrate and the adatoms and the subsequent entropy and second a long range elastic term E_{el} due to the crystal surface stress which is imposed by the presence of adatoms. In the framework of a continuous approach, both F_{chem} and E_{el} may be expanded with respect to the coverage θ , the η_j 's and their respective surface gradients. Let first write F_{chem} as follows:

$$F_{chem} = F_0 \cdot \int_S \int_S \left\{ \frac{\gamma_\theta}{2} [\nabla_s \theta]^2 + \frac{\gamma_\eta}{2} \sum_j [\nabla_s \eta_j]^2 + \hat{f}(\theta) \right\} d\mathbf{r} \quad (3)$$

We introduce here the adimensional free energy density written as

$$\hat{f} = A\theta^2 + E_2(\theta_1 - \theta) \sum_i \eta_i^2 - E_3\eta_1\eta_2 - E_4 \sum_i \eta_i^4 + E_5(\eta_1\eta_2)^2 + E_6 \sum_i \eta_i^6 \quad (4)$$

and the surface gradient $\nabla_s = [(\frac{\partial}{\partial x_1})^2 + (\frac{\partial}{\partial x_2})^2]$ where (x_1, x_2) are the surface coordinates along the (100) and (010) directions of the (001) cubic crystal surface. The F_0 and $\gamma_\eta, \gamma_\theta$ scalars are respectively the free energy

density constant and the amplitudes of the gradient term that both are adjusted to set the model domain boundary energy I to a realistic value, i.e., around $10 \text{ meV}/\text{\AA}$ (see Ref. [6,13]).

As the OP are supposed to describe the different variants of the internal layer structure, it is required that any symmetry operation relative to this structure should change the η_j 's leaving unchanged the \hat{f} quantity. For simplicity, the polynomial \hat{f} expansion is truncated after the sixth OP power and we focus on a case with only two OP's which is sufficient to study basic structures such as C2X2 and P2X1, well known from surface scientists (see Fig. 1 for the case of a (001) fcc surface).

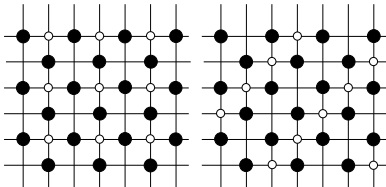


FIG. 1. : On a (001) fcc crystal surface (atoms of which are represented by full circles), the adatoms (empty circles) may arrange in a perfect C2X2 order (on the left hand side) or in a P2X1 order (on the right hand side). The direction [010] is indicated.

The C2X2 has 2 variants passing from one to the other by a $[1/2 \ 1/2 \ 0]$ surface vector translation. In our formalism, this structure can be represented by two \hat{f} minima for $\theta = 1$ and with either $\eta_1 = \eta_2 = 1$ or $\eta_1 = \eta_2 = -1$ depending on which variant is considered. The internal order P2X1 correspond to 2 orientational variants since the adatoms may arrange either along the direction $[110]$ or $[1\bar{1}0]$ and for each orientation there are two translational variants, passing from one to the other by a translation of $[1/2 \ 1/2 \ 0]$. This structure may correspond to four \hat{f} minima at $\theta = 1$ and with either $\eta_1 = \pm 1$ and $\eta_2 = 0$ or $\eta_2 = \pm 1$ and $\eta_1 = 0$. As a result of the P2X1 symmetries, the coupling coefficient E_3 in Eq. (4) must be zero. Minimizing the \hat{f} potential with respect to OP's for a given θ value gives two kind of minima, i.e., one disordered surface for which the whole set of OP is zero and some ordered surfaces for which the OP's have non zero values. The \hat{f} coefficients are adjusted such as plotting the \hat{f} potential after minimizing with respect to the OP's gives a double-well potential with two minima at $\theta = 0$ and $\theta = 1$.

The E_{el} energy is calculated by inverting the mechanical equilibrium equations, assuming a surface external force distribution \mathbf{P} . At the surface, we have

$$\sigma_{i,j}(\mathbf{r}, x_3 = 0) \cdot n_j = P_i(\mathbf{r}) \quad (5)$$

where n_j is a component of the surface normal $\mathbf{n} = [001]$ and the summation over subscript j is implicit. The crystal bulk stress, $\sigma_{i,j}(\mathbf{r}, x_3)$ is due to the crystal displacements $\mathbf{u}(\mathbf{r}, x_3)$ and it is given by the Hooke law:

$\sigma_{i,j} = \lambda_{i,j,k,l} \partial u_k / \partial x_l$. The fourth order tensor $\lambda_{i,j,k,l}$ gives the crystal elastic constants and for a cubic crystal symmetry, this tensor is composed with three non zero coefficients [14], namely $\lambda_{i,i,i,i} = C_{11}$, $\lambda_{i,i,j,j} = C_{12}$ and $\lambda_{i,j,i,j} = \lambda_{i,j,j,i} = C_{44}$. The bulk displacements fulfill the Lamé equation:

$$\lambda_{i,j,k,l} \frac{\partial^2 u_k}{\partial x_j \partial x_l} = 0 \quad (6)$$

The Eqs.(5,6) are inverted by writing the displacements as 2-dimensional Fourier transforms of which the Fourier components depend on both a surface wave vector $\mathbf{Q} = (q_1, q_2)$ and the deepness x_3 inside the bulk. As detailed in [8], it gives the surface elastic Green function $G_{i,l}(\mathbf{Q})$ as a linear function of the P_j Fourier transform, noted \tilde{P}_j . The total elastic energy of the system is given by an analytical expression in the Fourier space:

$$E_{el} = -1/2 \int_{x_3=0} \tilde{P}_i^* [G_{i,l}] \tilde{P}_l d\mathbf{Q} \quad (7)$$

Let note σ^0 the surface stress imposed by the adsorbed mono-layer. The induced force is simply obtained by deriving σ^0 with respect to the surface coordinates which gives:

$$P_i = \sum_{l=1,2} \frac{\partial \sigma_{il}^0}{\partial x_l} \quad (8)$$

For simplicity, we choose to focus on a case where $P_3 = 0$ which means that σ^0 can be reduced to a 2×2 matrix. This stress tensor is expanded with respect to the local coverage θ and the OP's, i.e., η_1 and η_2 . On one hand, if no anisotropy appears in the layer structure which is the case for a disordered layer or when there is no orientational variants, e.g., the C2X2, then we write $\sigma^0(\mathbf{r}) = \sigma^{00}\theta(\mathbf{r})$ with $\sigma_{12}^{00} = \sigma_{21}^{00} = 0$ and $\sigma_{11}^{00} = \sigma_{22}^{00} = \Lambda$. On the other hand, if there are orientational variants, one must add a correction to $\sigma^{00}\theta(\mathbf{r})$ and we propose to write

$$\sigma^0(\mathbf{r}) = \sigma^{00}\theta(\mathbf{r}) + \sum_{j=1,2} \sigma^{0j}\eta_j(\mathbf{r})^2 \quad (9)$$

This expansion holds when the OP's correspond one-to-one to the structure orientations which is the case in our representation of the P2X1 order. We focus on the P2X1 orientational variant where first adatom neighbors are placed along the $[110]$ direction (Fig. 1). Let note Λ_1 and $\Lambda_{\bar{1}}$, the amplitudes of the stress along $[110]$ and $[1\bar{1}0]$, respectively. We have $|\Lambda_1| > |\Lambda_{\bar{1}}|$ because of the proximity of first adatom neighbors which reveals the internal structure anisotropy. After performing a suitable rotation, the stress tensor is written in the repair $[100] \times [010]$ as follows: $\sigma_{11}^0 = \sigma_{22}^0 = \Lambda$ and $\sigma_{12}^0 = \sigma_{21}^0 = \mu$ where $\Lambda = 0.5(\Lambda_1 + \Lambda_{\bar{1}})$ and $\mu = 0.5(\Lambda_1 - \Lambda_{\bar{1}})$. We now identify to the Eq. (9) for a perfect P2X1 ordered domain with the suitable orientational variant which gives

the same expression σ^{00} as for the C2X2 phase but with non-zero off-diagonal coefficients for the σ^{01} tensor: $\sigma_{12}^{01} = \sigma_{21}^{01} = \mu$. Same can be done with the other P2X1 orientational variant and it gives $\sigma_{12}^{02} = \sigma_{21}^{02} = -\mu$. As Λ_1 and $\Lambda_{\bar{1}}$ are assumed to have same sign which means that a dilation (or compression) occurs in both directions $[110]$ and $[\bar{1}\bar{1}0]$, then we note that $|\mu| < |\Lambda|$.



FIG. 2. : Phase separation final state on a (001) Copper crystal surface with $\Lambda = 40 \text{ mJ/m}^2$ (defined in the text) for a C2X2 (first row) at $\theta_0 = 0.25$ (on the left), $\theta_0 = 0.5$ (in the middle), $\theta_0 = 0.75$ (on the right hand side) and for a P2X1 (second row) with $\mu = 0.9\Lambda$ at $\theta_0 = 0.38$ (on the left), $\theta_0 = 0.5$ (in the middle) and $\theta_0 = 0.75$ (on the right hand side). The gray scale enhances the different variants of the layer structures. The direction $[010]$ is indicated.

Let remind the model parameters: $I=10 \text{ meV/\AA}$, $\Lambda = 40 \text{ mJ/m}^2$ ($\Lambda = 0.25 \text{ eV/\AA}^2$) and the elastic constants of Copper $C_{11} = 1.683$, $C_{12} = 1.221$ and $C_{44} = 0.757$ which unit is 10^{11} J/m^3 (see Physics Handbooks). The Eqs. (1,2) are integrated with a finite space and time element method. The space unit cell is $1 \text{ nm} \times 1 \text{ nm}$ and the time increment is around 1ns. The kinetics starts from a uniform coverage $\theta = \theta_0$ and a uniform random distribution of OP's between -1 and 1.

On a (001) cubic crystal surface, the ordering process is shown to lead to a steady state with different mesoscopic patterns according to the coverage and the internal structure (see Fig. 2). Because of the crystal cubic symmetry and the mono-layer internal structure, the final state differ from the one predicted in Refs. [5–7]. Nevertheless the space correlation function of the final state, i.e., $\langle \theta(\mathbf{r} + \tau)\theta(\mathbf{r}) \rangle$ exhibits a characteristic wave length which decreases exponentially with the boundary energy I which confirms the predictions established in [5,6].

For a perfect C2X2 internal structure, no internal anisotropy is induced. Only the symmetries of the underlying crystal play a role in the patterning. At $\theta_0 = 0.25$, the phase separation kinetics yields a nanostructure of square shaped island arranged in raft along either the $[100]$ or the $[010]$ directions that are the elastic soft directions of the Copper surface. The two translational

variants are identified with two different shades of grey. For $\theta_0 = 0.5$, a labyrinthine nanostructure occurs with two kinds of wall according to the translational variants of the ordered phase. For $\theta_0 = 0.75$, the situation is not the counterpart of a surface with $\theta_0 = 0.25$ (see Fig. 2) as one would expect from a simple phase separation. Some anti-phase boundaries (APB) due to the coexistence of different order appear as trenches between the neighboring domains. The present theoretical results about a (001) Copper surface with a C2X2 mono-layer may be compared with what is experimentally observed in [1,2] with the STM analysis of the N/Cu(001) system. The atomic precision of the STM enhanced adatom missing rows which our model can not capture because of the coarse-graining. In the experiments, those missing rows occur every 5.2 nm along both $[100]$ and $[010]$ directions and thus the adatom layer appears as an assembly of square shaped islands with 5.2 nm size. According to Leible *et al.* [1], those missing rows are due to the lattice parameter mismatch between the bulk lattice constants of Cu_3N and the (001) Copper surface unit cell. Nevertheless if one accepts to consider the islands separated by missing rows as a single domain then the final state patterns enhanced by the STM experiments are very similar to the ones shown in the first row of Fig. (2), for different coverage. Indeed, the C2X2 structure with missing rows might be consider as a non-perfect C2X2 with no internal anisotropy as the perfect C2X2.

The P2X1 order implies a layer internal anisotropy, i.e., $\mu \neq 0$. In the second row of Fig. (2), it is shown that the patterns strongly differ from the C2X2 case. The domains appear as tips size of which are oriented along specific directions. The weaker is $(1 - \mu/\Lambda)$, i.e., the stronger is the internal anisotropy, the thinner are the tips and their sizes tends to be align with either $[110]$ or $[\bar{1}\bar{1}0]$. The second row of Fig. (2) shows the different patterns according to the coverage for $\mu = 0.9\Lambda$ which is close from the μ upper limit. The tips with different variant do not branch to each other because of the APB and the growth of some domains may be stopped by their neighbors with different orientations.

The anisotropy factor of a cubic crystal is given by the combination of the elastic constants $\chi = C_{11} - C_{12} - 2C_{44}$ (see Ref. [14]). The crystal is isotropic for $\chi = 0$ which is the case for amorphous material as glasses. For example, Copper and Gold χ 's are negative ($\chi_{Cu} = -1.0$, $\chi_{Au} = -0.5$), and Chromium and Niobium χ 's are positive ($\chi_{Cr} = +1.8$, $\chi_{Nb} = +0.5$). The case $\chi < 0$ as for Copper is described above while for a positive χ , the soft elastic directions of the crystal surface are $[110]$ and $[\bar{1}\bar{1}0]$ instead of $[100]$ and $[010]$ for a negative χ . For $\chi > 0$, our calculations showed that the internal anisotropy of a P2X1 layer does not modify the preferential orientations of domains due to the crystal symmetries, i.e., $[110]$ and $[\bar{1}\bar{1}0]$. Only the shape of the domains is changed at low coverage passing from square islands arranged in raft along $[110]$ and $[\bar{1}\bar{1}0]$ when $\mu = 0$ to long tips aligned in same directions when $\mu > 0$. A C2X2 layer deposited

on a cubic crystal with $\chi > 0$ gives same patterns as a P2X1 layer with $\mu = 0$: the steady surfaces are same as the first row pictures of the Fig. 2 after performing a rotation of 45 degrees around the [001] direction, i.e., the domain sizes are aligned with either [110] or $[\bar{1}\bar{1}0]$ instead of [100] or [010].

In summary, it is proved that the patterning which is yielded by the ordering of atomic mono-layer onto crystal surface is controlled by the symmetries of both the internal layer structure and the underlying crystal. Our results about the ordering of a C2X2 layer on a Copper surface are in a good agreement with the experiments. The method we used in the present paper is a powerful tool to predict the nanostructures that may be constructed experimentally with different crystal and different adsorbate.

In an other field of research, i.e., the magnetic films, a similar approach have been used by A. Cebers [15] who enhanced the different patterns that may be yielded from the interplay between the magnetic domain boundary energy and the long range magnetic dipolar energy, according to the external magnetic field. To that respect, we believe that a model extension including both the magnetic and the elastic energy terms should be possible to describe the magneto-striction which may occur on a crystal surface by depositing magnetic compounds.

Heinemann, (1995), pp. 54-55.

[15] A. Cebers, Phys. Rev. E **61**, 700 (2000).

-
- [1] F. M. Leible *et al.*, Phys. Rev. B **47**, 15865 (1993).
 - [2] H. Ellmer *et al.*, Surf. Sci. **476**, 95 (2001).
 - [3] T.W. Fishlock *et al.*, Surf. Sci., **445**, 47 (2000).
 - [4] M. Sotito and B. Croset, Surf. Sci. **461**, 78 (2000).
 - [5] V.I. Marchenko, Sov. Phys. JETP **54**, 605 (1981).
 - [6] O.L. Alerhand, David Vanderbilt *et al.*, Phys. Rev. Lett. **61**, 1973 (1988).
 - [7] Kwok-On Ng and David Vanderbilt, Phys. Rev. B **52**, 2177 (1995).
 - [8] L. Proville, Phys. Rev. B, 045139 (to be published 15 October 2001).
 - [9] J.D. Gunton *et al.*, *Phase Transitions and Critical Phenomena*, Academic Press, Vol. 8, Eds. C. Domb and J.L. Lebowitz, (1983) p. 269.
 - [10] A.J. Bray, Advances in Physics, **43**, 357 (1994).
 - [11] A.G. Khachatryan, *Theory of Structural Transformations in Solids*, chap. 7, Ed. Wiley-Interscience, New-York (1983).
Yunzhi Wang, L.Q. Chen and A.G. Khachatryan, in *Computer in Material Science*, vol. **308** NATO ASI Series, Eds. H.O. Kirchner, L.P. Kubin and V. Pontikis (1996) p. 325.
 - [12] A. Zangwill, *Physics at surfaces*, Cambridge University Press, (1988) p. 380.
 - [13] B. Croset *et al.*, submitted to Phys. Rev. Lett. (2001).
 - [14] E.M. Lifshitz and L. D. Landau, *Theory of Elasticity* (Theoretical Physics, Vol.7), 3rd edition Butterworth-